DOI: 10.24352/UB.OVGU-2017-005 TECHNISCHE MECHANIK, 36, 3, (2016), 190 - 198
submitted: May 22, 2016

Mesh Independency Analyses and Grid Density Estimation for Ventricular Assist Devices in Multiple Reference Frames Simulations

G.B. Lopes Jr., L.C. Gómez, E.G.P. Bock

The evolution of mechanical circulatory supports has been essential to improve life quality for heart disease patients. The ventricular assist devices (VAD) developments, for example, incorporated computational engineering in its process to reach more robust devices. A concern in VAD developments still being the dynamics of the flow inside blood pumps, and so computational fluid dynamics (CFD) has being studied and applied to these developments processes. In CFD, many aspects become relevant and essential, especially in turbulent flows in which numerical and physical instabilities may cause divergence or false results. In order to reduce the numerical error and guarantee an appropriate fluid domain representation, mesh independency is essential to reach reasonable results. In this context this work is presented, as support for grid density estimation from precision analysis, since accuracy to real data is not numerically relevant in mesh independency determination. Ansys Fluent was used for performing 36 simulations with different grid densities for a VAD prototype, applying multiple reference frames (MRF) methodology. Grid densities incorporate the number of elements in a reference frame and the geometric scale of a VAD, what creates comparison parameters for use in other fluid flow simulations using MRF applied to VADs. In each reference frame, although, this density might be different for optimization of computational costs and to reach trustful results. Another concern felt in the fluid-fluid interface between the two reference frames, keeping concordance and soft transitions between the frames meshes, aiming to reduce locally numerical error propagations. The impeller Reynolds number is around 2800 and the inlet Reynolds number is 317. Despite the low Reynolds number, turbulence may occur and standard k-e model is applied for turbulent flow analyses. The blood is considered as Newtonian and incompressible fluid due to velocities and fluid deformations expected, thus mean values are applied for density and effective viscosity: 1059kg/m³ and 0,004Pa.s. Simulations are compared in global analysis, verifying the pressure difference between inlet and outlet, and in specific analysis, observing the fluid flow behavior, aiming for changeless. Both analyses are based on numerical precision, what means the simulations are compared mutually, changing the grid density scenarios. Results suggest independency of mesh size from 13 million of elements, with variance coefficient around 0,7%, and grid density parameters are purposed as references for mesh disposal in VAD simulations in same conditions. The use of 318,43 elements per mm³ and 210,14 elements per mm³ are sufficiently to assure mesh size independency for non-inertial (near the rotor) and inertial frames, respectively. The purpose of this work is to reach a grid density parameter for applying in future similar simulations and analyze mesh influence on the specific results of the blood flow inside the prototype VAD. The goals are to reach and as conclusion a minimum grid density is purposed for VAD simulations applying MRF in the similar or lower impeller Reynolds numbers, and probably for higher impeller Reynolds numbers as well.

1 Introduction

Cardiovascular disease cases have constantly increased over last decades on the global scale. Every year, 660 thousand new patients, older than 45 years old, suffer from heart failure in United States (Thumberg et al., 2010), and the number of patients with cardiac diseases may reach 23 million in 2030 (Mozaffarian et al., 2015). Analysing transplant indicators (U.S. transplants, 2015), the transplant evolution from 1988 to 2014 indicates a mean survival rate of 87% for patients who received the transplanted organs. In addition, around 3400 new candidates were in the waiting list for heart transplant, and 727 patients were removed from the waiting list, just in 2014, for death or worsening their medical conditions.

In this context, mechanical circulatory support and Ventricular Assistance Devices (VAD) are developed aiming to completely recover or increase life expectancy for specific purposes. Consequently, heart failure patients assisted with those mechanisms experience improvements in life quality (La Franca et al., 2013). In view of the importance, VAD development have been including more efficient methodologies, as numerical simulations, improving in three classes of pumps in the last two decades (Thumberg et al., 2010).

In 2014, the Food and Drugs Administration (FDA) published its guidance for numerical analysis during medical devices development, indicating this new exigency (FDA, 2014). Several studies were conducted for numerical simulations of blood flow (Fraser et al., 2011; Fraser et al., 2012; Song et al., 2003; Zhang et al., 2013) applying

Computational Fluid Dynamics (CFD) techniques to analyze the blood flow behaviour and several numerical issues, for example, turbulence models to be applied.
This work analyzes mesh size independency and indicates a grid density parameter to be used in VAD simulations for Multiple Reference Frames (MRF). Despite some comments about meshes and their sizes in VAD numerical simulations (Fraser et al., 2012; Zhang et al., 2013, for example), the grid density factor is not commented, nor details for mesh size independency. So, this study is justified, since this is an essential step in a numerical simulation using CFD techniques.

2 Material and Methods

The numerical simulations presented in this paper were carried out with an Implantable Centrifugal Blood Pump (ICBP), shown in Figure 1 and previously studied by Bock et al. (2011).

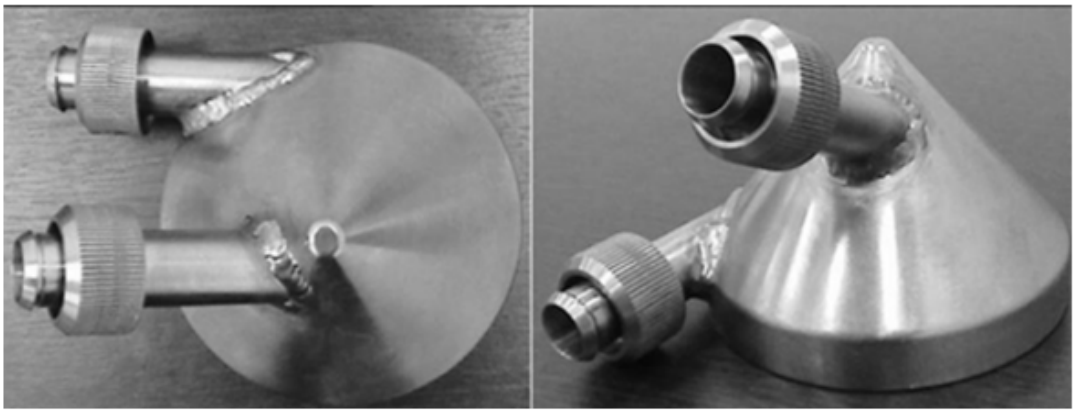

Figure 1: Analyzed VAD, studied by Bock et al. (2011).

Multiple Reference Frames

The Multiple Reference Frames (MRF) is a numerical strategy to simulate non-inertial domains when the transient behavior is not relevant for the desired analyses. The MRF is widely used in pump or mixing steady-state simulations to reduce the computational costs in transient simulations or dynamic mesh use. This methodology consists in creating at least two different domains (sub-domains), with different reference velocities, connected by a fluid-fluid interface.
Pump simulations usually consider a non-inertial domain close to the rotor and inertial domain between the stator and the fluid-fluid interface. The simulations conducted in this paper use the MRF strategy. Thus, each domain was simulated with its own reference velocity, while the fluid-fluid interface adjusts the reference changes between each domain.

The Fluid Domain

The fluid domain represents the regions filled by the mathematically modeled fluid using the CFD numerical procedures. The present work defines two different fluid sub-domains, where the MRF numerical strategy is applied.
The first sub-domain was non-inertial and represented by an inner fluid region situated near the pump rotor. The second fluid sub-domain consists in the external region of the fluid regarding the pump rotor, inlet and outlet pump regions, and it is an inertial domain.
Besides these two sub-domains, inlet and outlet regions were also set in extended cylindrical fluid regions. These regions are artificially added to the real fluid domain, because this “far distance” reduces the influence of numerical assumed boundary conditions at the inlet and outlet surfaces on the blood pump structures.

Mesh Adequacy

The mesh adequacy is based on proximity and curvature, which means that the mesh was generated giving priority to the wall and curve regions. The growth rate applied in the several scenarios varies from 5% to 100%, indicating the most refined and the coarsest meshes, respectively.
The fluid-fluid interface is set as another priority aiming to solve any discontinuity from the non-inertial and inertial meshes. Beside the adequacy parameters, tetrahedrons are generated, and a continuous growth rate was applied for each mesh.

Conservation Equations

The Ansys Fluent software simulates the blood flow inside the pump for creating the different scenarios. The continuity equation, considering incompressible turbulent flow, Reynolds Decomposition ($V_i = \overline{V}_i + v'_i$), and Average Procedure is given by Eq. (1).

$$\frac{\partial \overline{V}_i}{\partial x_i} = \overline{\frac{\partial v'_j}{\partial x_j}} = 0 \tag{1}$$

Since the simulations are considered as isothermal, the momentum conservation equation, for incompressible turbulent flow with constant Newtonian viscosity, and without field forces that are not relevant for the problem, is written as Eq. (2)

$$\frac{\partial \rho \overline{V}_i}{\partial t} + \frac{\partial \rho \overline{V}_i \overline{\boldsymbol{V}}}{\partial x_j} = -\frac{\partial \overline{p}}{\partial x_j} + \frac{\partial \boldsymbol{\tau}_{ji}}{\partial x_j} \tag{2}$$

Where $\overline{V}$ is the local instantaneous mean velocity magnitude, v' is the fluctuation velocity, $\overline{\boldsymbol{V}} = \overline{V}_x \boldsymbol{i} + \overline{V}_y \boldsymbol{j} + \overline{V}_z \boldsymbol{k}$ is the vector of mean velocities, and $\boldsymbol{\tau}$ is the stress tensor defined by Eq. (3), based on the Boussinesq theory, considering a Newtonian fluid and the Stokes hypothesis.

$$\boldsymbol{\tau}_{ji} = (\mu + \mu_t)\left(\frac{\partial V_i}{\partial x_j} + \frac{\partial V_j}{\partial x_i}\right) - \frac{2}{3}\rho\kappa\delta_{ji} \tag{3}$$

where μ is the molecular viscosity, μ_t is the eddy viscosity, κ is the turbulent kinetic energy, and δ_{ji} is the Kronecker delta.

The turbulence models applied were the standard $\kappa - \varepsilon$ and $\kappa - \omega$. The Eqs. from 4 to 9 are solved to compute the following turbulent parameters: turbulent kinetic energy (κ), turbulent dissipation rate (ε) and the specific dissipation rate (ω).

For the $\kappa - \varepsilon$ model: Eqs. (4) and (5).

$$\frac{\partial(\rho\kappa)}{\partial t} + \frac{\partial(\rho \overline{V}_i \kappa)}{\partial x_i} = \frac{\partial}{\partial x_j}\left[\left(\mu + \frac{\mu_t}{\sigma_\kappa}\right)\frac{\partial \kappa}{\partial x_j}\right] - \rho\epsilon - \overline{\rho v'_i v'_j}\frac{\partial(\overline{V}_i)}{\partial x_j} \tag{4}$$

$$\frac{\partial(\rho\varepsilon)}{\partial t} + \frac{\partial(\rho \overline{V}_i \varepsilon)}{\partial x_i} = \frac{\partial}{\partial x_j}\left[\left(\mu + \frac{\mu_t}{\sigma_\varepsilon}\right)\frac{\partial \varepsilon}{\partial x_j}\right] - C_{1_\epsilon}\frac{\varepsilon}{\kappa}\overline{\rho v'_i v'_j}\frac{\partial(\overline{V}_i)}{\partial x_j} - C_{2_\epsilon}\rho\frac{\varepsilon^2}{\kappa} \tag{5}$$

In Eqs. (4) and (5) the closure standard coefficients are set: $C_{1_\epsilon} = 1{,}44$, $C_{2_\epsilon} = 1{,}92$, $\sigma_\kappa = 1{,}0$ and $\sigma_\varepsilon = 1{,}3$. The turbulent viscosity is calculated by Eq. 6 from the Boussinesq approximation.

$$\mu_t = 0{,}09.\rho.\frac{\kappa^2}{\epsilon} \tag{6}$$

For the $\kappa - \omega$ model: Eqs. From (7) to (9).

$$\frac{\partial(\rho\kappa)}{\partial t} + \frac{\partial(\rho \overline{V}_i \kappa)}{\partial x_i} = \frac{\partial}{\partial x_j}\left[(\mu + \sigma^*\mu_t)\frac{\partial \kappa}{\partial x_j}\right] - \rho\beta^*\omega k - \overline{\rho v'_i v'_j}\frac{\partial(\overline{V}_i)}{\partial x_j} \tag{7}$$

$$\frac{\partial(\rho\omega)}{\partial t} + \frac{\partial(\rho \overline{V}_i \omega)}{\partial x_i} = \frac{\partial}{\partial x_j}\left[(\mu + \sigma\mu_t)\frac{\partial \omega}{\partial x_j}\right] - \rho\beta\omega^2 - \alpha.\frac{\omega}{\kappa}.\overline{\rho v'_i v'_j}\frac{\partial(\overline{V}_i)}{\partial x_j} \tag{8}$$

$$\mu_t = \alpha^*.\rho.\frac{\kappa}{\omega} \tag{9}$$

In Eqs. 7 and 8, the closure coefficients for the standard model are considered: $= 5/9$, $\sigma^* = \sigma = 0{,}5$, $\beta = 3/40$, and $\beta^* = C_\mu = 0{,}09$. The coefficient $\alpha^* = C_\mu/\beta^*$ may have different values, when β^* and C_μ have divergent empirical values. Some authors (including Wilcox, 1994) indicates $\alpha^* = 1$. This value was adopted for high-

Reynolds numbers by the software, but when the turbulent Reynolds number was lower, the Eq. 10 was applied (Ansys Inc, 2011), where $Re_t = \rho.\kappa/\mu.\omega$.

$$\alpha^* = \left(\frac{0{,}024 + Re_t/6}{1 + Re_t/6}\right) \tag{10}$$

Boundary and Initial Conditions

The velocity was fixed on inlet, according to volumetric flow rate for each scenario, and outflow conditions were applied on the outlet, in which condition velocity and pressure are extrapolated from the interior (diffusive flux is null), and a mass balance correction is applied. These conditions and the geometrical far position of the inlet and outlet regions guarantee interference from the boundaries is not overlapped until solving the flow.
Non-slip velocity condition was set at the walls, and for turbulence modeling the wall treatment varied from wall functions (in the coarse meshes) and near-wall model approaches (in the refined meshes), solving the turbulent conservation equations in the near-wall elements. The transition between the two methods of near-wall resolution is set by the software, according to the first element distance (Ansys Inc, 2012). Figure 2 illustrates the idea.

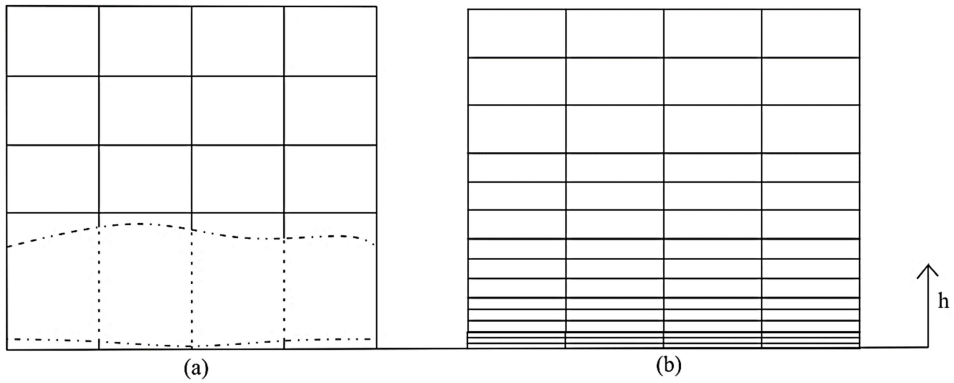

Figure 2: Near-wall treatment: (a) wall functions; (b) near-wall model approaches.

The turbulent initial conditions were based on the Komogorov relations for the turbulent parameters, as indicated by Ansys Inc (2011). So, the turbulent kinetic energy equation is based on the turbulent intensity ($I_t = v'/\overline{V}$), where $v' = \sqrt{(2/3)\,\kappa}$ and $\overline{V}$ is taken as a reference velocity (V_{ref}), usually equal to the inlet velocity. Thus, Eq. (11) is applied.

$$\kappa_\infty = 1.5.\left(V_{ref}.I_t\right)^2 \tag{11}$$

The turbulent intensity, I_t, is given by Eq. (12), for best practice recommendation (14), when its value is under 10%.

$$I_t = 0.16.Re^{-1/8} \tag{12}$$

The turbulent kinetic energy dissipation could be evaluated by the equation for the Komogorov scale length, adopting $\upsilon = \upsilon_t$ and replacing Eq. 6 on it, resulting on Eq. 13.

$$\epsilon_\infty = \frac{C_\mu^{3/4}.\kappa_\infty^{1,5}}{l} \tag{13}$$

The length scale, l, is also another best practice estimation, being based on Eq. 14 (14), where L is a characteristic length, adopted as the diameter of the inlet tube.

$$l = l_m = 0.07.L \tag{14}$$

Besides these parameters, ω was evaluated by Eq. 15.

$$\omega_\infty = \frac{\epsilon_\infty}{\beta^*\kappa_\infty} = \frac{C_\mu^{3/4}.\kappa_\infty^{0,5}}{0.07.\beta^*.L} \tag{15}$$

Scenarios

Simulations were performed in three different scenarios:

- First, the rotor rotation was set to 800 rpm, and the volumetric flow rate equal to 0,508 l/min was adopted, measured in experiments (Bock et al., 2011)). 36 simulations were performed for initial results with different grid densities, and the $\kappa - \varepsilon$ model was applied for turbulence.
- The second scenario aimed to analyze the critical grid densities, in which mesh size independency was observed in the first scenarios. The four densest meshes were tested for 2200 rpm and 6,93 l/min. In this scenario, it was analyzed the influence of wall in the worse condition tested in the experiments (Bock et al., 2011).
- In the last scenario tested, the same conditions of the second scenario were applied, but the turbulent model. The $\kappa - \omega$ model was set to analyze the influence of another turbulence model which has improvements in wall effect modeling (Wilcox, 1994).

Comparison

In all scenarios tested, the pressure difference between the inlet and outlet ports is used to compare the numerical results to the experimental data from Bock et al. (2011). Despite the importance of the comparison, no accuracy analyses were performed. This work focuses on precision to reach mesh size independency and grid density estimation.

3 Results

The total number of elements varied from 930980 to 17778903, used in the 36 simulations for scenario 1; in scenario 2 and 3, the number of elements varied from 15107776 to 17778903, performing 4 simulations for each scenario. The inertial frame assumed from 272508 to 5610948 elements, what resulted in around 11,96 and 246,27 elements per mm³ as grid densities, respectively. For the non-inertial frame, grid densities varied from 20,32 to 375,45 elements per mm³, all tested in scenario 1.

Scenario 1

The simulations performed in the first scenario show that from 13 million elements, the precision of the simulation results became practically stable and this tendency was more evident from the use of 15 million of elements, as presented in Figure 3.

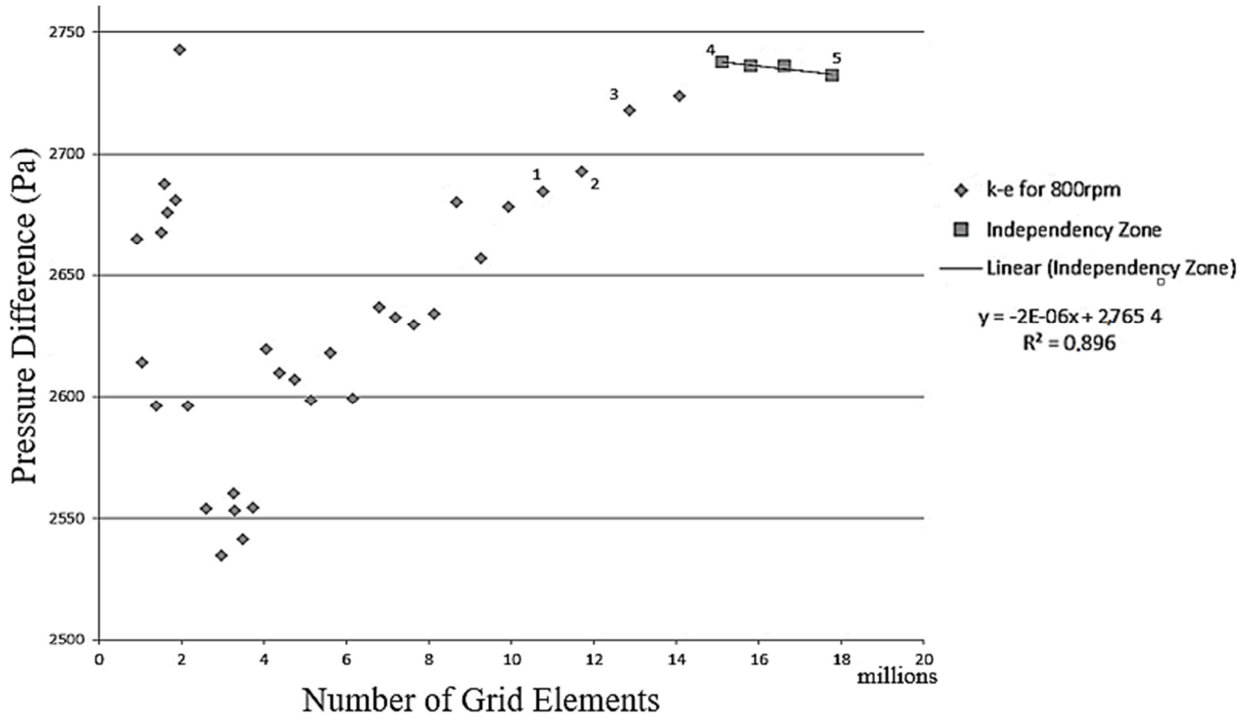

Figure 3: Global analysis for grid density using MRF in scenario 01: k-e model and 800rpm

Note that the variable used for establishing the mesh size independency in Figure 3 was the pressure difference between the inlet and outlet sections. Analyzing the results of Figure 3, one of the first simulations with a coarse mesh showed a similar pressure difference value to those obtained for the fine meshes (15 million of elements and more). However, as seen in Figure 3, a slight increase of the mesh size resulted in considerable differences in the pressure difference, reaching the smallest values of this variable for approximately 3 million elements. And so the pressure differences increased until reaching an almost constant value about 2740 Pa.
In order to analyze the mesh size independency, a linear interpolation curve was plotted in Figure 3 between the points 4 and 5, respectively. Considering, the simulations from 3 to 5, represented in Figure 4, the standard deviation between the pressure differences was around 8.0940, while the variance coefficient was 0.2964%. Analyzing only the simulations from 4 to 5, the standard deviation equaled to 2.2161 and the variance coefficient reduced to 0.0810%, respectively. These small differences indicate that for these meshes is obtained the desired independency of the simulation results from the applied mesh.
Aiming to analyze the specific behavior due to the grid density in scenario 1, Figure 4 presents the velocity streamlines, starting from 50 equally spaced points in inlet section for simulations between 1 and 5, as presented in Figure 3.

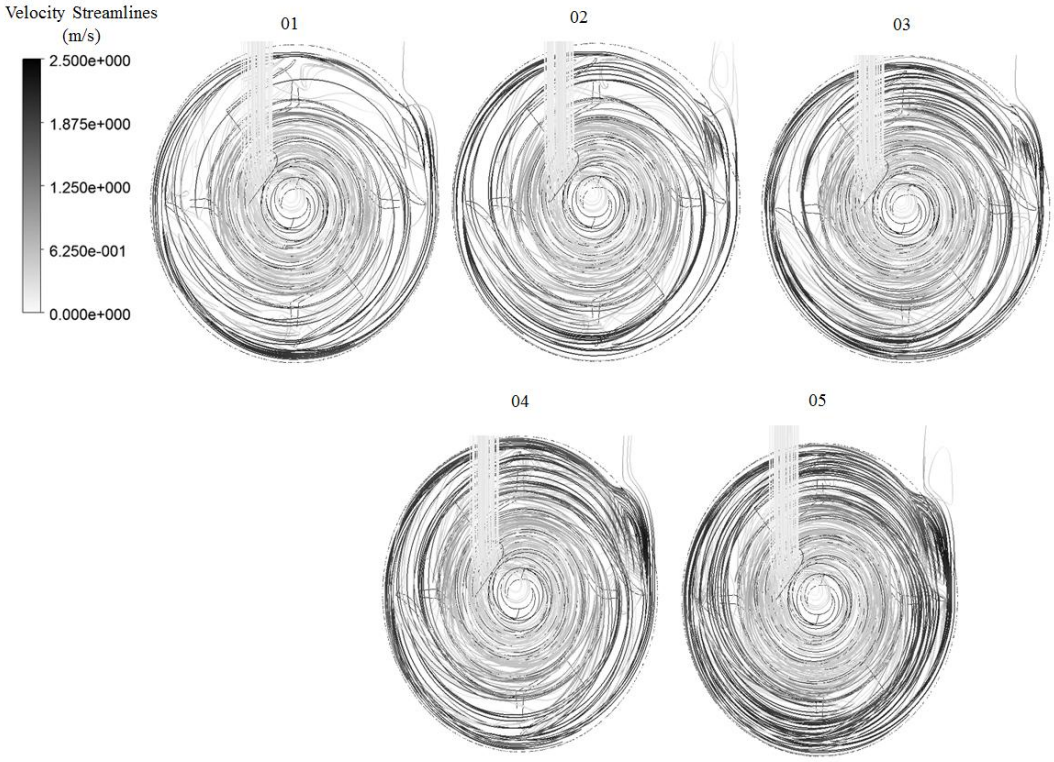

Figure 4: Streamlines comparisons for scenario 01 in five different grid densities.

The simulations 4 and 5 show very similar results according to the streamlines behavior. The simulation 3 was also similar, but the streamlines could not completely represent the flow near the rotor exit, even when similar to the cases to 4 and 5. On the other hand, simulations 1 and 2 could not represent the same results as in 4 and 5, probably due to the "poor density" in the non-inertial frame.

Scenario 2 and 3

In scenarios 2 and 3, the variance coefficient increased to 0.8234% and 2.1879%, respectively, for the same grid densities used in the simulations from 4 to 5. Although these values represent more than 10 times the variance coefficient presented in scenario 1, they indicate small variations of the predicted pressure differences. In figure 5, the pressure difference is presented for comparison of the global results for these two scenarios.

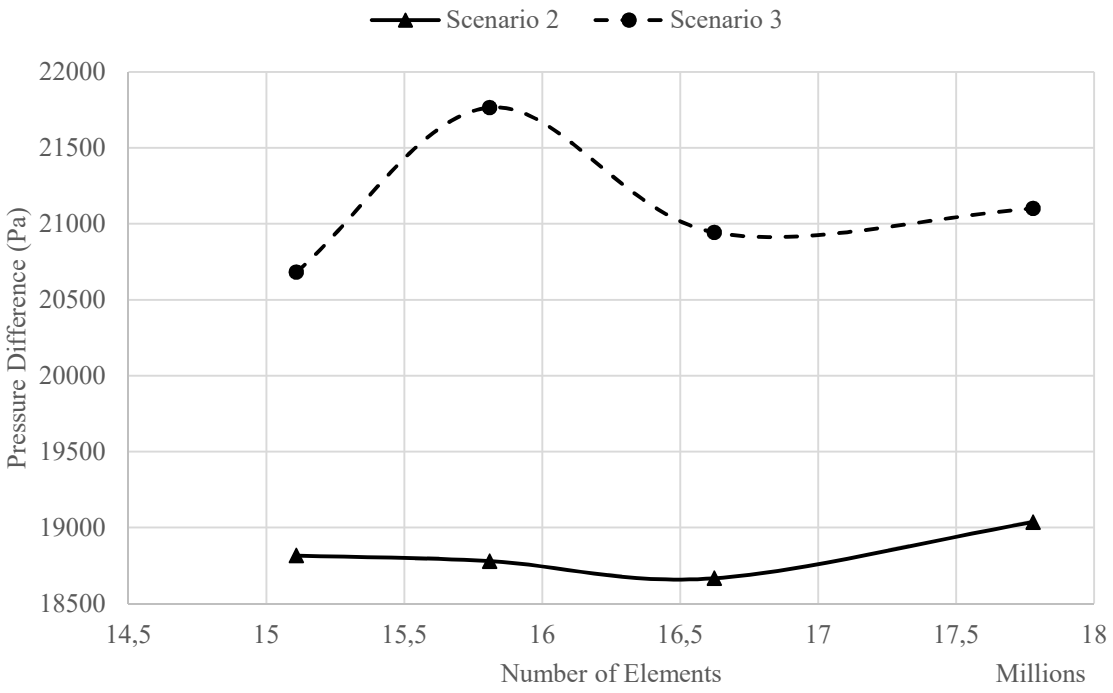

Figure 5: Comparison between scenario 2 and 3 for global results

These differences can be explained due to the increase of both quantities: the rotation velocity from 800 to 2000 rpm; and the volumetric mass flow from 0.508 l/min to 6.93 l/min. These two operational variables commonly lead to an increase on flow turbulence parameters which can alter the behavior of the main flow variables. Velocity distribution near the rotor can be analyzed in Figure 6.

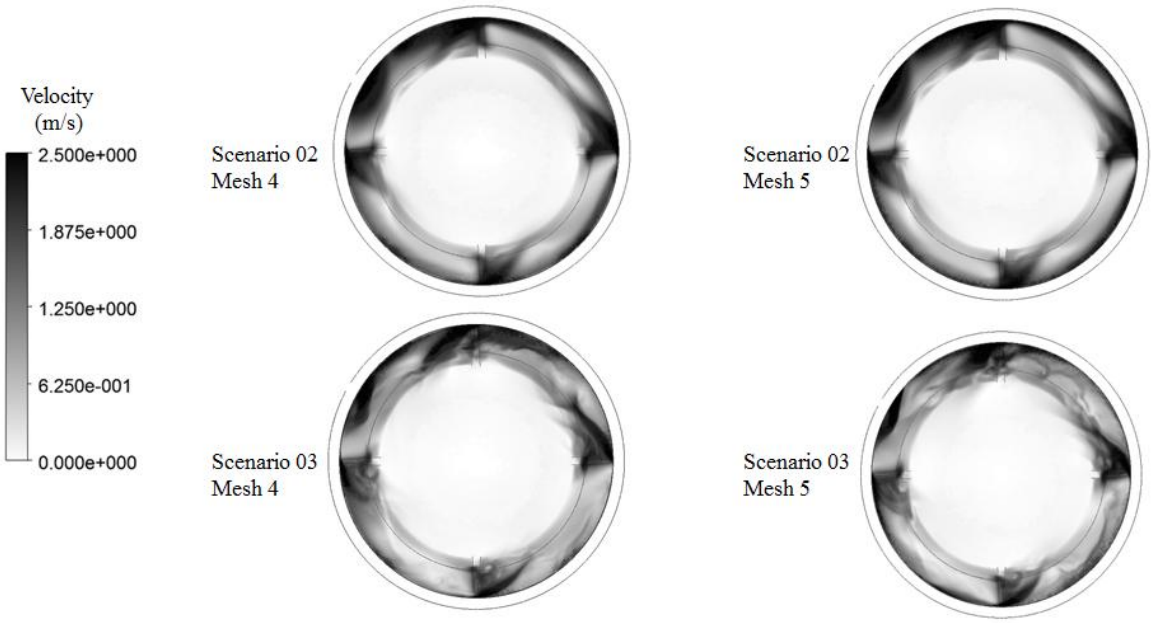

Figure 6: Velocity distribution near the rotor for mesh 4 and 5 detached in Figure 4, for Scenarios 2 and 3.

A similar behavior can be observed with slight difference presented in Scenario 3, probably due the turbulence effect. Aiming to analyze this, the eddy viscosity is shown in Figure 7, the values presented are also similar as distributed in both Scenarios.

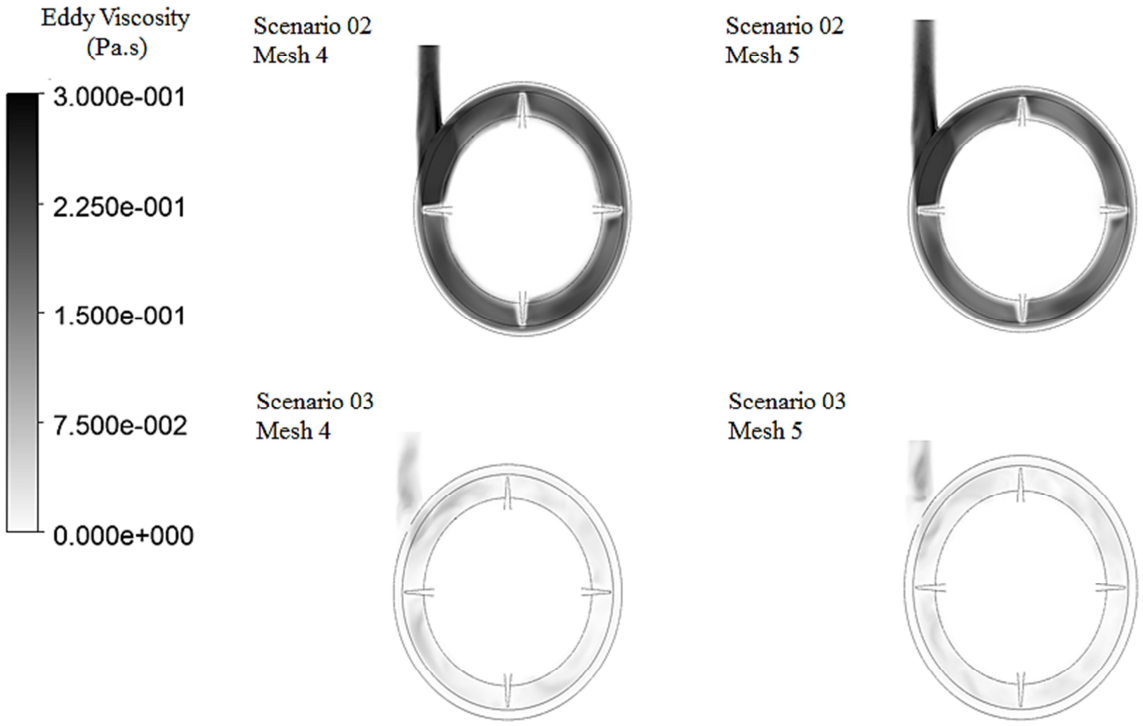

Figure 7: Eddy viscosity behavior for mesh 4 and 5 detached in Figure 5, for Scenarios 2 and 3.

4 Conclusions

There are few and subtle differences from point 4 to point 5 in the presented results, which are irrelevant for the global flow results. On the other hand, while the mesh used in the simulation 4 consist of 15,107,776 elements, the mesh used in the simulation 5 incorporated 2,671,127 more elements. This mesh size difference is relevant to the simulation time.

The influence of turbulence is preponderant in numerical analyses of VADs. The use of size independent meshes resulted in non-variation of parameters and global pressure differences, what indicate an optimized point. So the numerical errors associated to turbulence influence stabilized, as well as all flow quantities, and the simulation time is the lowest possible in an application.

Therefore, the use of 318.43 elements per mm^3 and 210.14 elements per mm^3 or more, for non-inertial (near the rotor) and inertial frames, respectively, guarantee the mesh size independency for simulations using multiple reference frames in numerical modeling for ventricular assistance devices.

References

Ansys Inc.: *Ansys Fluent Theory Guide*. Ansys Inc. publication, release 14.0, 2011.

Ansys Inc.: *Ansys Fluent User's Guide*. Ansys Inc. publication, release 14.5, 2012.

Bock E, Antunes P, Leao T, Uebelhart B, Fonseca J, Leme J, Utiyama B, da Silva C, Cavalheiro A, Filho DS, Dinkhuysen J, Biscegli J, Andrade A, Arruda C: Implantable Centrifugal Blood Pump With Dual Impeller and Double Pivot Bearing System: Electromechanical Actuator, Prototyping, and Anatomical Studies. *Artificial Organs*. 2011; 35:437–442.

Food and Drug Administration. Reporting of Computational Modelling Studies in Medical Device Submissions. Draft Guidance for Industry and Food and Drug Administration Staff. U.S. Department of Health and Human Services, 2014 (on line publication).

Fraser, K.H., Taskin, M.E., Griffith, B.P., Wu, Z.J.: The Use of Computational Fluid Dynamics in The Development of Ventricular Assist Devices. *Medical Engineering & Physics*. 2011; 33: 263-80.

Fraser, K.H., Zhang, T., Taskin, M.E., Griffith, B.P., Wu, Z.J.A: Quantitative Comparison of Mechanical Blood Damage Parameters in Rotary Ventricular Assist Devices: Shear Stress, Exposure Time and Hemolysis Index. *Journal of Biomechanical Engineering*. 2012; 134, 2012: 081002-1 - 11.

LaFranca E., Iacona, R., Ajello, L., Sansone, A., Caruso, M., Assennato, P.: Heart Failure and Mechanical Circulatory Assist Devices. *Global Journal of Health Science*. 2013; 5(5): 11-19.

Mozaffarian D., Benjamin E.J., Go A.S., Arnett D.K., Blaha M.J., Cushman M., de Ferranti S., Després J.-P., Fullerton H.J., Howard V.J., Huffman M.D., Judd S.E., Kissela B.M., Lackland D.T., Lichtman J.H., Lisabeth L.D., Liu S., Mackey R.H., Matchar D.B., McGuire D.K., Mohler E.R. 3rd, Moy C.S., Muntner P., Mussolino M.E., Nasir K., Neumar R.W., Nichol G., Palaniappan L., Pandey D.K., Reeves M.J., Rodriguez C.J., Sorlie P.D., Stein J., Towfighi A., Turan T.N., Virani S.S., Willey J.Z., Woo D., Yeh R.W., Turner M.B.: Heart disease and stroke statistics - 2015 update: a report from the American Heart Association. American Heart Association Statistics Committee and Stroke Statistics Subcommittee, 2015 (online publication).

Organ Procurement and Transplantation Network. Data reports: U.S. transplants. U.S. Department of Health and Human Service. accessed in 2015 (online publication).

Song, X., Wood, H.G., Day, S.W., Olsen, D.B.: Studies of Turbulence Models in a Computational FluidDynamics Model of a Blood Pump. *Artificial Organs*. 2003; 27(10): 935-37.

Thumberg, C.A., Gaitan, B.D., Arabia, F.A., Cole, D.J., Grigore, A.M.: Ventricular Assist Device Today and Tomorrow. Review Article in *Journal of Cardiothoracic and Vascular Anesthesia*. 2010 Aug; 24(4): 656-80.

Wilcox, D.C.: *Turbulence Modelling for CFD*, DCW Industries, Inc., 1994.

Zhang, J., Zhang, P., Fraser, K.H., Griffith, B.P., Wu, Z.J.: Comparison and Experimental Validation of Fluid Dynamic Numerical Models for a Clinical Ventricular Assist Device. *Artificial Organs*. 2013; 37(4): 380-89.

Address: R. Randolfo Borges Júnior, 1250, Institute of Technology and Exact Sciences, Federal University of Triangulo Mineiro, Uberaba-MG, Brazil.
Corresponding author email: lopesjunior.gb@gmail.com

Acknowledgments:
The authors are grateful to Bock et al. (2011) for supplying data for the developed analyses. The authors also acknowledge CNPQ, FAPESP, and FAPEMIG for financial support.